Hindawi
Geofluids
Volume 2020, Article ID 8892720, 15 pages
https://doi.org/10.1155/2020/8892720

Research Article

Sealing Form and Failure Mechanism of Deep In Situ Rock Core Pressure-Maintaining Controller

Nianhan Wu ,[1] Heping Xie,[2,3] Ling Chen ,[1] Mingzhong Gao ,[2,3] and Cong Li[2,3]

[1]*School of Mechanical Engineering, Sichuan University, Chengdu 610065, China*
[2]*State Key Laboratory of Hydraulics and Mountain River Engineering, College of Water Resource and Hydropower, Sichuan University, Chengdu 610065, China*
[3]*Guangdong Provincial Key Laboratory of Deep Earth Sciences and Geothermal Energy Exploitation and Utilization, Institute of Deep Earth Sciences and Green Energy, College of Civil and Transportation Engineering, Shenzhen University, Shenzhen 518061, China*

Correspondence should be addressed to Ling Chen; chenlingscu@scu.edu.cn

Received 13 August 2020; Accepted 20 October 2020; Published 16 November 2020

Academic Editor: Zhijie Wen

The mechanical properties of deep rocks change nonlinearly in an in situ pressure environment, so standard cores cannot be used as real samples for deep rock mechanics research. Therefore, obtaining an in situ pressure core is essential. However, the existing pressure-maintaining cores cannot overcome the sealing capacity limit, largely due to the lack of consideration of sealing theory and experimental verifications of pressure-maintaining controllers. Therefore, this paper explores the sealing form and failure mechanism of pressure-maintaining controllers. The sealing state transition, pressure leakage, deformation failure theory, and test method for a pressure-maintaining controller are determined. Through theoretical analysis and experiments, (1) a seal-form discrimination method based on the chimeric curve is proposed to obtain the pressure seal conversion trend; (2) the leakage rate is exponentially related to the initial pressure, which confirms the pressure leakage principle of the pressure-maintaining controller; and (3) based on deformation failure theory for pressure-maintaining controllers, the failure mode and deformation trend are obtained through a destructive limit pressure experiment. The research results provide a theoretical basis and experimental support for improving pressure coring in deep rock and obtaining pressure cores at deep positions to construct a new conceptual system of deep in situ rock mechanics.

1. Introduction

Since the 20th century, large-scale exploitation has led to the depletion of shallow Earth resources, and the exploitation of resources from the deep Earth has become a significant strategic approach worldwide [1]. However, the existing shallow engineering theories and methods based on standard cores have failed to effectively guide the extraction of deep mineral resources [2]. The basic mechanical parameters of rocks display linear and even nonlinear changes with increasing depth [3]. Zhang et al. performed in situ stress recovery test research on coal and rock masses at different depths in the Ping coal mine area of China and found that the elastic modulus changes nonlinearly with depth [4, 5]. Kang et al. performed a theoretical analysis of the support of coal roadways and found that when the roadway burial depth is deeper than 800 m, the secondary support mechanism based on traditional rock mechanics is invalid [6–8]. At present, research on deep rock characteristics is focused on atmospheric cores. Regardless of how deep the samples are taken, they are almost all obtained under the condition of relieving the in situ pressure without considering the influence of the real in situ pressure environment [9]. The release of the in situ pressure will have an irreversible impact on the physical and mechanical properties of the rock [10]. Therefore, obtaining in situ pressure cores is important for developing a new theory of deep in situ rock mechanics and advancing pressure-maintaining coring techniques.

At present, research in the fields of Earth science, oil and gas exploration, engineering geology, civil engineering, water

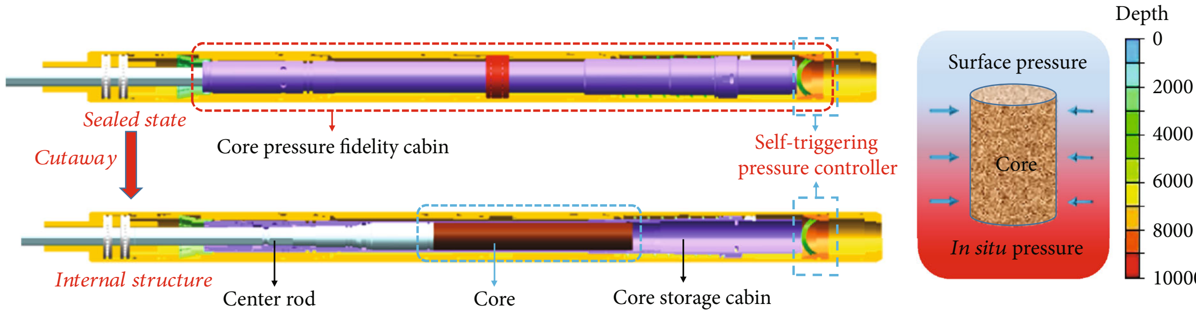

Figure 1: In situ pressure-maintaining coring of rock.

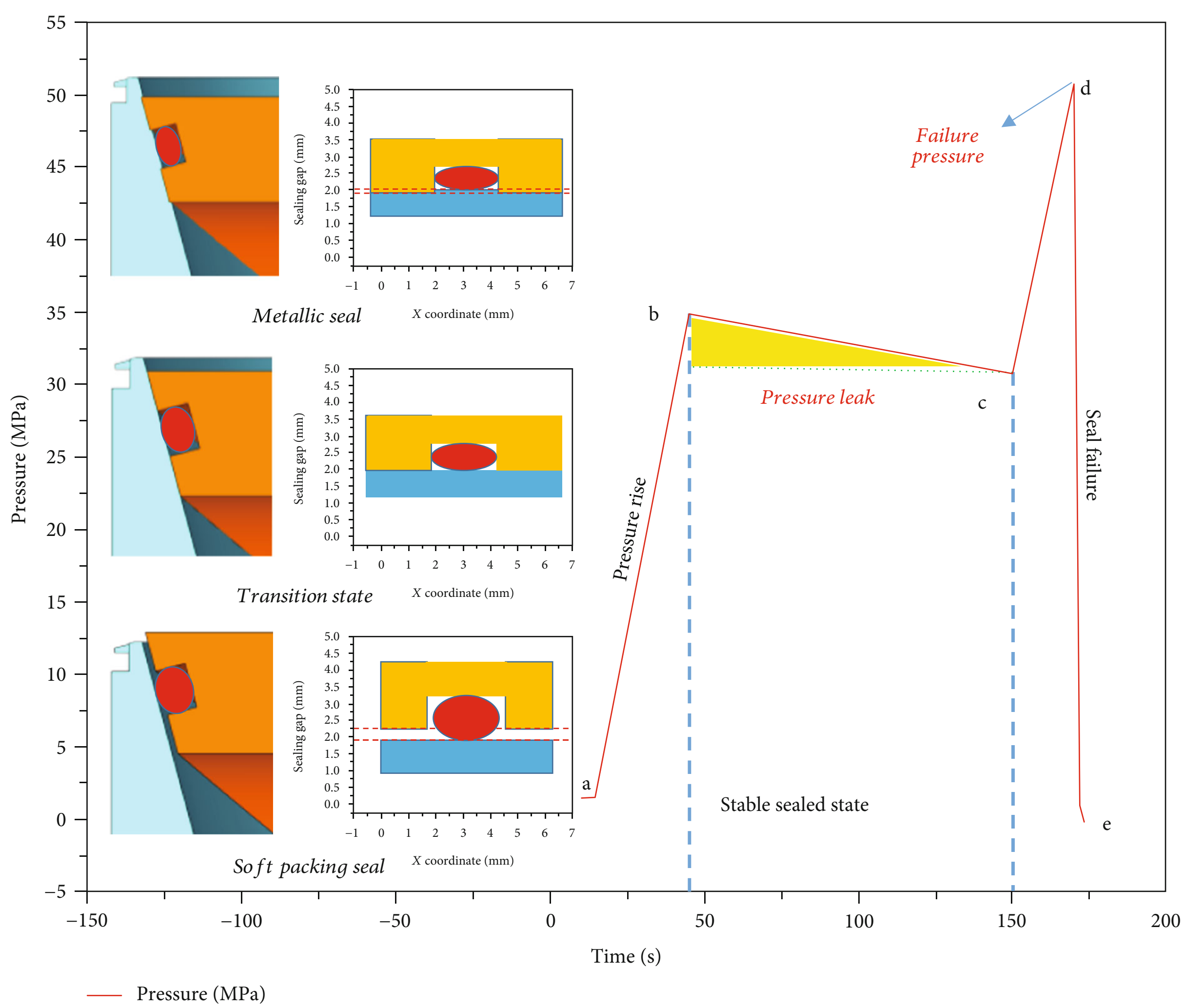

Figure 2: Sealing state and pressure change process.

conservation engineering, mining science, and other disciplines relies on drilling and coring technology to obtain cores [9]. Due to the failure to seal the core pressure in traditional land drilling, the in situ pressure is released when a core is extracted. Additionally, the existing mature pressure-maintaining coring technology is generally applied in deep-sea drilling for the production of gas hydrates [11–15]. As shown in Figure 1, the key part of the pressure-coring system is the pressure-maintaining controller, and the maximum sealing capacity of the pressure-maintaining controller determines the maximum working pressure of the entire pressure-coring device. At present, "Pressure Core Sampler (PCS)" [11, 12] provides the largest pressure-maintaining capacity in deep-sea coring, reaching 70 MPa, which cannot meet

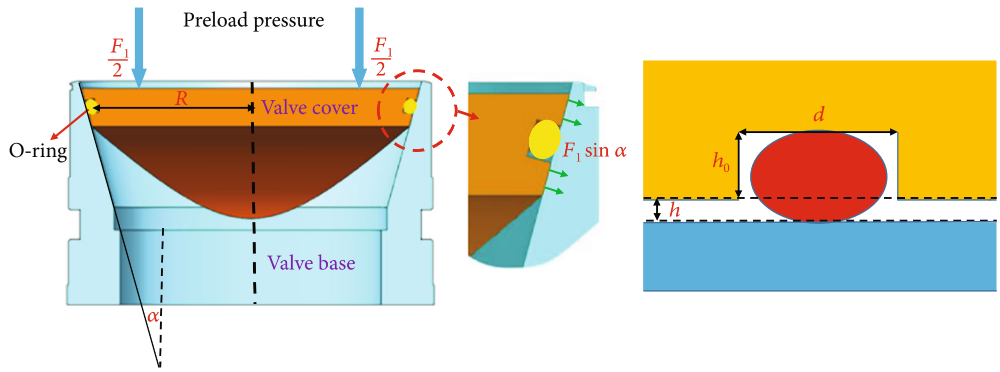

FIGURE 3: Sealing structure and dimension parameters of a pressure-maintaining controller.

the in situ pressure requirements of deep-sea cores below 7000 m. Moreover, it is impossible to perform pressure coring for hard rock in deep land areas. The maximum working pressure of the coring device is limited by the pressure-maintaining controller. Therefore, improving the pressure-sealing capacity of the pressure-maintaining controller is a prerequisite for pressure coring in the deep parts of the Earth (10000 m).

The pressure-maintaining capacity is closely related to the initial sealing stability, pressure leakage rate, and ultimate pressure resistance capacity of the pressure-maintaining controller. Many scholars have studied practical applications of pressure-maintaining controllers and performed analyses and tests of the pressure-maintaining ability of devices.

1.1. Study of the Maximum Pressure-Maintaining Capacity in Practical Applications. Many countries around the world have researched the pressure-maintaining capacity of coring devices. In 1983, the ODP organization in the United States developed the second-generation PCB coring device-PCS, which was sealed with a ball valve and had a working pressure close to 70 MPa [13]. This equipment has been used to extract pressure-maintaining combustible ice from the Blake Ridge [14]. The hydrate coring equipment system (HYACE), funded by the EU marine science and technology project, has successfully collected pressure-maintaining cores and can be used at an approximate in situ pressure of 35 MPa [15]. The pressure-maintaining coring tool PTCs [16] developed by JOGMEC in Japan can work under a pressure of 30 MPa [17]. Actual drilling applications have verified that the system is effective in sandstone sediments.

1.2. Studies of Sealing Theory and Test Methods for the Pressure-Maintaining Capacity. Many scholars have studied the sealing form and failure mechanism of pressure-maintaining controllers. Zhang et al. performed simulation and experimental research on flexible and rigid sealing mechanisms and proposed a simplified finite element model for flexible seals. Through simulation calculations and experiments, the theory was verified to have a practical guiding value [18]. Liu et al. performed a theoretical analysis of the leakage and deformation of the O-ring in the axial soft seal model based on use in practical problems [19]. Farfán-Cabrera et al. reconstructed a high-pressure environment to test sealing performance under different working conditions.

TABLE 1: Sealing parameters of the pressure-maintaining controller.

Parameter	Numerical value	Variable
$r_1(m)$	1.5×10^{-3}	O-ring radius
$h_0(m)$	2.5×10^{-3}	Seal groove depth
$d(m)$	3×10^{-3}	Seal groove width
$R(m)$	5×10^{-2}	Seat diameter
E_o (MPa)	10×10^{3}	Elastic modulus of O-ring
R_m (MPa)	12	Shear strength of O-ring
α	15°	Angle of sealing surface

Through an appearance assessment of the sealing surface, the best sealing condition was obtained [20]. Peng et al. performed experimental research on a remote sealing method for vacuum leakage. The remote measurement method was used to detect leakage in vacuum tubes [21]. The study mentioned above did not consider the pressure-maintaining capacity of the coring system and lacked a testing method for the pressure-maintaining controller; thus, no theoretical or experimental guidance was provided for the optimization of pressure-maintaining systems.

Therefore, this paper presents a pressure-sealing principle and failure theory for a coring system based on a pressure-maintaining controller. According to the pressure capacity of the coring system [22, 23], the sealing state and environment reconstruction test system are designed for a pressure-maintaining controller. In situ pressure environment simulation experiments were conducted from the perspectives of seal-form conversion, the pressure leakage rate, and the ultimate pressure resistance capacity to preliminarily verify the proposed theory. The results of this paper provide a theoretical basis and experimental support for improving the pressure capacity of deep rock coring systems and can be used to establish a technical means for obtaining deep in situ pressure cores.

2. Pressure Seal and Form Conversion Principles

2.1. Sealing Principle and Pressure Change Analysis. Under the condition of extremely high pressure, there are three

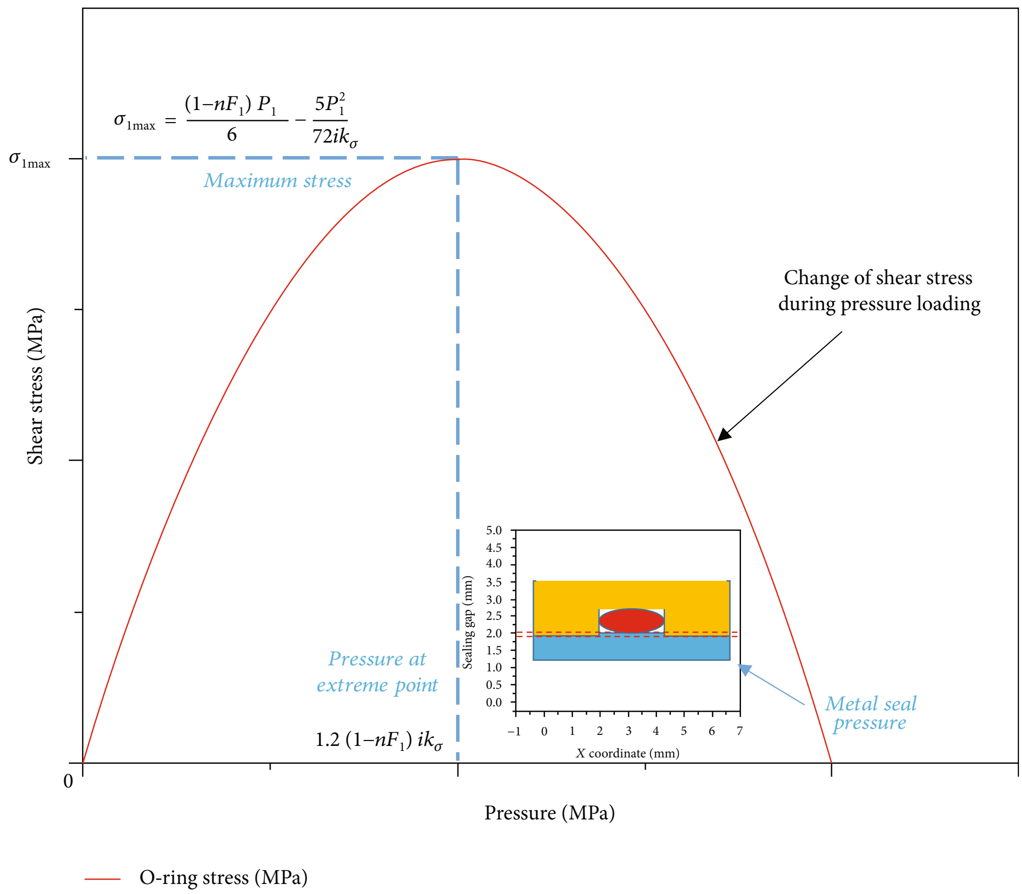

Figure 4: Shear stress variation for the O-ring.

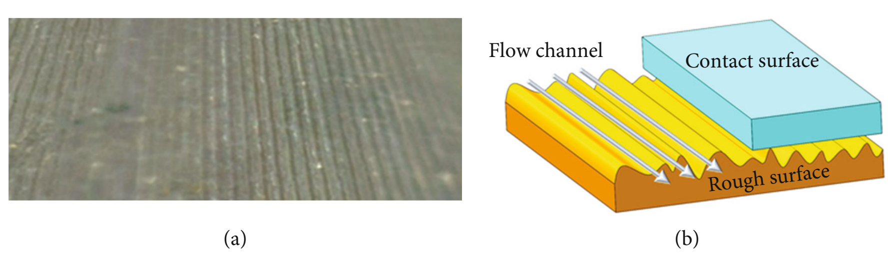

Figure 5: Schematic diagram of a liquid flow channel on the contact surface. (a) Scanning diagram of a valve seat metal surface. (b) Schematic diagram of a flow channel on the contact surface.

key sealing processes involved in the process from sealing to failure. At first, when the pressure increases gradually, the sealing form changes from O-ring soft seal to metal hard seal. Then, when the pressure-maintaining controller is stable, there will be a certain amount of pressure leakage. Finally, the pressure-maintaining controller will produce plastic deformation and damage under the limit pressure condition. These three processes affect the sealing form conversion and pressure-maintaining accuracy and ultimately withstand the voltage capacity of the pressure-maintaining controller. The sealing ability of the pressure-maintaining controller is also closely related to these three sealing performance parameters.

As shown in Figure 2, the simulated pressure curve reflects the changes in the sealing state of the pressure-maintaining controller with the pressure. Point A denotes the initial sealing stage, point B denotes the normal working pressure of the pressure-maintaining controller, and point D denotes the ultimate withstandable voltage capacity of the pressure-maintaining controller. Along line A-B, the internal environmental pressure of the pressure-maintaining controller gradually increases. When the environmental pressure reaches position B, the pressure-maintaining controller enters a stable sealing state, but at this time, a certain amount of pressure leakage will inevitably occur. As the pressure continues to increase, the internal environmental pressure of the pressure-maintaining controller exceeds the maximum working pressure. When the failure pressure is reached, the seal of the pressure-maintaining controller will fail, and the

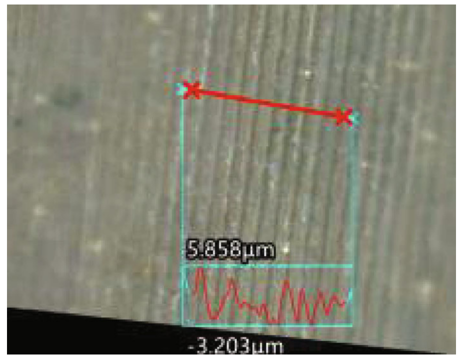

(a)

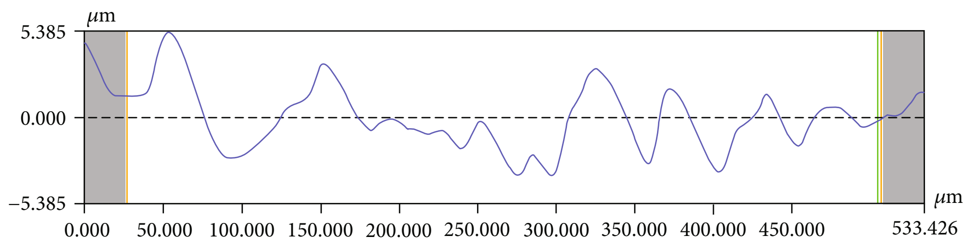

(b)

FIGURE 6: Scanning diagram of the contact surface contour curve. (a) Surface scanning diagram. (b) Surface roughness profile curve.

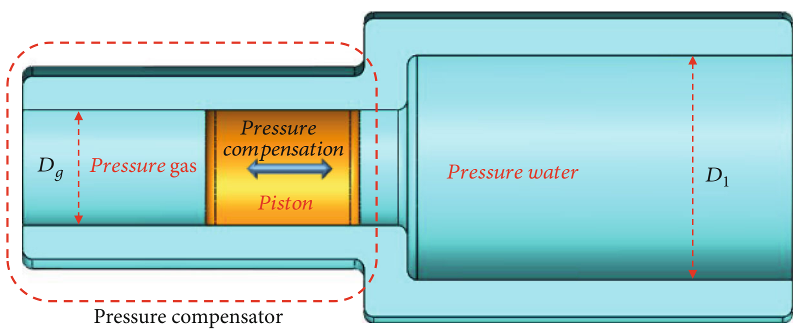

FIGURE 7: Schematic diagram of the pressure compensation mechanism.

sealing pressure will rapidly decrease to the external environment pressure.

2.2. Mechanism of Sealing Form Conversion. As shown in Figure 3, when the pressure-maintaining controller reaches the sealing state, a conical sealing surface is formed between the valve cover and the valve seat. The O-ring deforms and seals under the extrusion of the conical surface. The sealing form of the pressure-maintaining controller will change at different pressures. The initial sealing state involves the soft O-ring seal, which gradually transforms into a metal hard seal with increasing pressure [24].

When there is no environmental pressure, the O-ring will deform under the prepressure $F_1(N)$. The deformation variable is S. The contact surface angle of the pressure-maintaining controller is α. The elastic modulus of the selected fluororubber O-ring is iE_o (GPa), and i is the elastic modulus coefficient of fluororubber at different compression levels [25]. $L_1(m)$ is the length of the sealing groove, and $d(m)$ is the width of the sealing groove. The O-ring shape variable can be expressed as shown in the following formula:

$$S = \frac{F_1 \sin \alpha}{iE_o L_1 d}. \tag{1}$$

Since the sealing ring is a three-dimensional intersecting curve, the length of the sealing groove is determined by the inner diameter $R(m)$ of the pressure-maintaining controller and the angle α of the contact surface. Therefore, the length of the sealing groove can be expressed as follows:

$$L_1 = 2k_\alpha \pi R. \tag{2}$$

In formula (2), k_α is the correction factor for the length of the sealing groove. When α is 15°, k_α is approximately 1.3. When the pressure begins to change, the valve cover will be subjected to the hydraulic force P_1 (MPa) acting on the valve

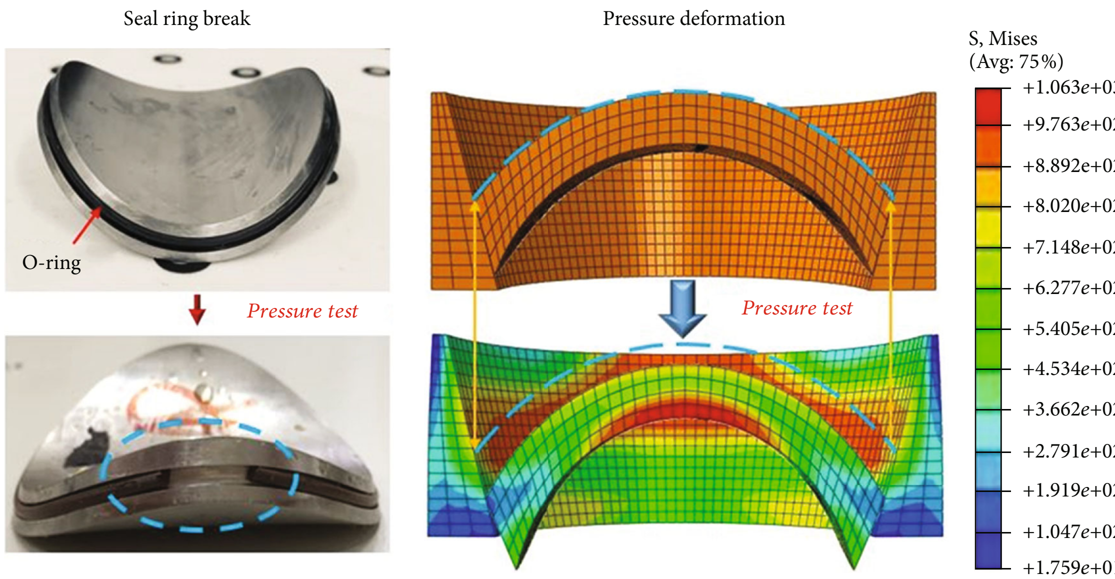

Figure 8: Deformation and damage of a pressure-maintaining controller.

seat, and the pressure $F_2(N)$ on the O-ring is as follows:

$$F_2 = \left(\pi R^2 P_1 + F_1\right) \sin \alpha. \tag{3}$$

The initial radius of the fluororubber O-ring is $r_1(m)$, and the depth of the sealing groove is $h_0(m)$. Then, the distance $h(m)$ between the valve cover and the valve seat can be expressed as follows:

$$\begin{aligned} h &= 2r_1 - h_0 - \frac{\left(\pi R^2 P_1 + F_1\right) \sin \alpha}{iE_o L_1 d} \\ &= 2r_1 - h_0 - \frac{\left(\pi R^2 P_1 + F_1\right) \sin \alpha}{2k_\alpha \pi R i E_o d}. \end{aligned} \tag{4}$$

According to formula (4), when the pressure gradually increases, the gap between the valve cover and the metal surface of the valve seat will gradually decrease. When the ambient pressure reaches P_2 (MPa), the valve cover contacts the valve seat, and P_2 (MPa) is given by the following formula:

$$P_2 = \frac{2k_\alpha i E_o d(2r_1 - h_0)}{R^2 \sin \alpha} - \frac{F_1}{\pi R^2}. \tag{5}$$

At a normal temperature, the shear strength R_m (MPa) of the fluororubber O-ring is 12 MPa. In the soft sealing stage, the shear stress σ_1 of the O-ring is calculated as follows:

$$\begin{aligned} \sigma_1 &= \int_0^{2\pi} \frac{\partial \theta R h P_1}{2\pi R d} = \frac{hP_1}{d} \\ &= \frac{(2r_1 - h_0)P_1}{d} - \frac{\left(\pi R^2 P_1 + F_1\right) \sin \alpha P_1}{2k_\alpha \pi R i E_o d^2}. \end{aligned} \tag{6}$$

Formula (6) indicates that when $\sigma_{1\ \max}$ (MPa) is less than R_m (MPa), the soft seal of the pressure-maintaining controller remains effective. When the metal surface is in contact, the shear stress is 0, and the pressure-maintaining controller enters the metal seal state.

The sealing parameters of the pressure-maintaining controller are shown in Table 1. The shear stress of the O-ring has an inverse quadratic parabolic relationship with the pressure. The corresponding functional diagram is shown in Figure 4.

Figure 4 shows that when the initial pressure is 0, the shear stress of the seal ring is 0. With increasing pressure, the shear stress first increases and then decreases. When the seal becomes a metal seal, the shear stress is approximately 0. According to formula (6), when the pressure reaches the extreme point, the shear stress reaches a maximum.

3. Pressure Leakage and Failure Mechanism for a Pressure-Maintaining Controller

When a pressure-maintaining controller enters the soft sealing state or metal sealing state and the environmental pressure no longer changes, the internal pressure can vary; nevertheless, it decreases at a specific rate [26]. As shown in Figure 5, the metal surface of the pressure-maintaining controller is not completely flat. Based on the machining tool path, the surface will have a certain roughness characteristic. Therefore, from a microperspective, when the pressure-maintaining controller achieves a stable seal, there will still be a specific liquid flow channel in the middle of the contact surface [27].

At high pressure, a certain amount of leakage $\Delta Q(L)$ will occur in the pressure-maintaining tank, which will lead to decreases in the liquid quantity $Q(L)$ in the container and in the pressure P_0 (MPa). According to the Bernoulli equation, the pressure P_1 (MPa) in the vessel satisfies the

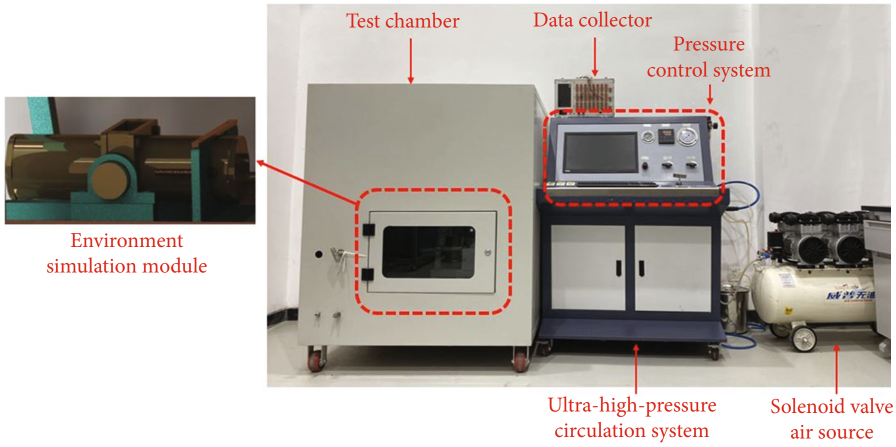

Figure 9: Physical diagram of the experimental device.

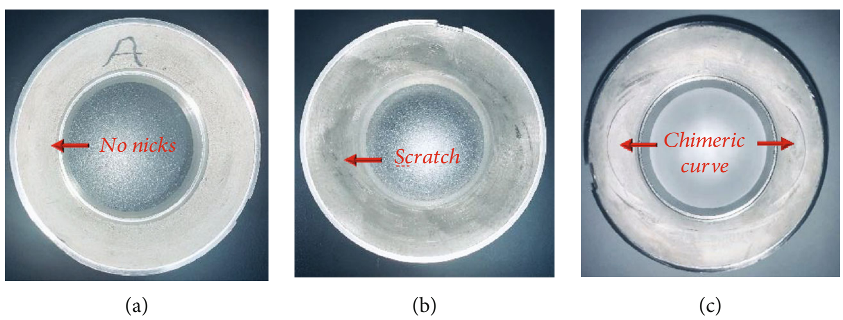

Figure 10: Experimental results based on the seal-form chimerism curve. (a) No chimerism at low pressures. (b) Sealing transition stage. (c) High-pressure chimerism stage.

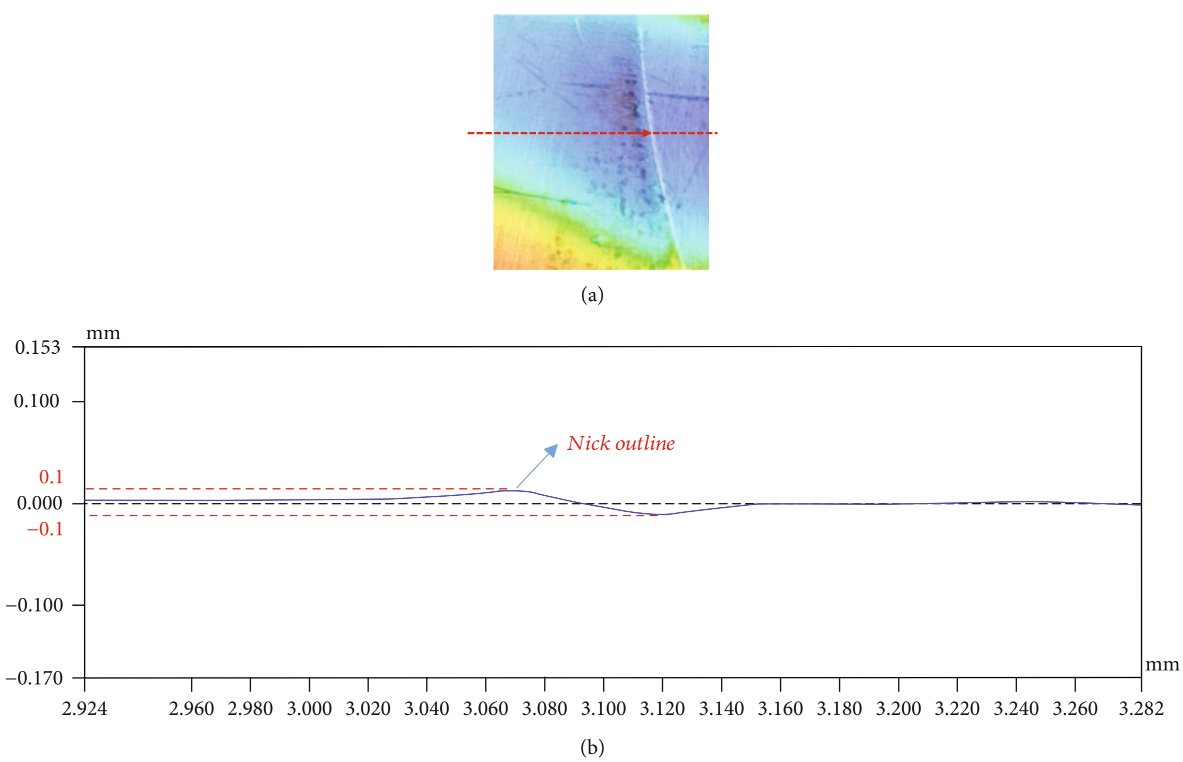

Figure 11: Three-dimensional scanning measurement of the chimeric curve. (a) Scanning nephogram. (b) Scratch depth and contour curve.

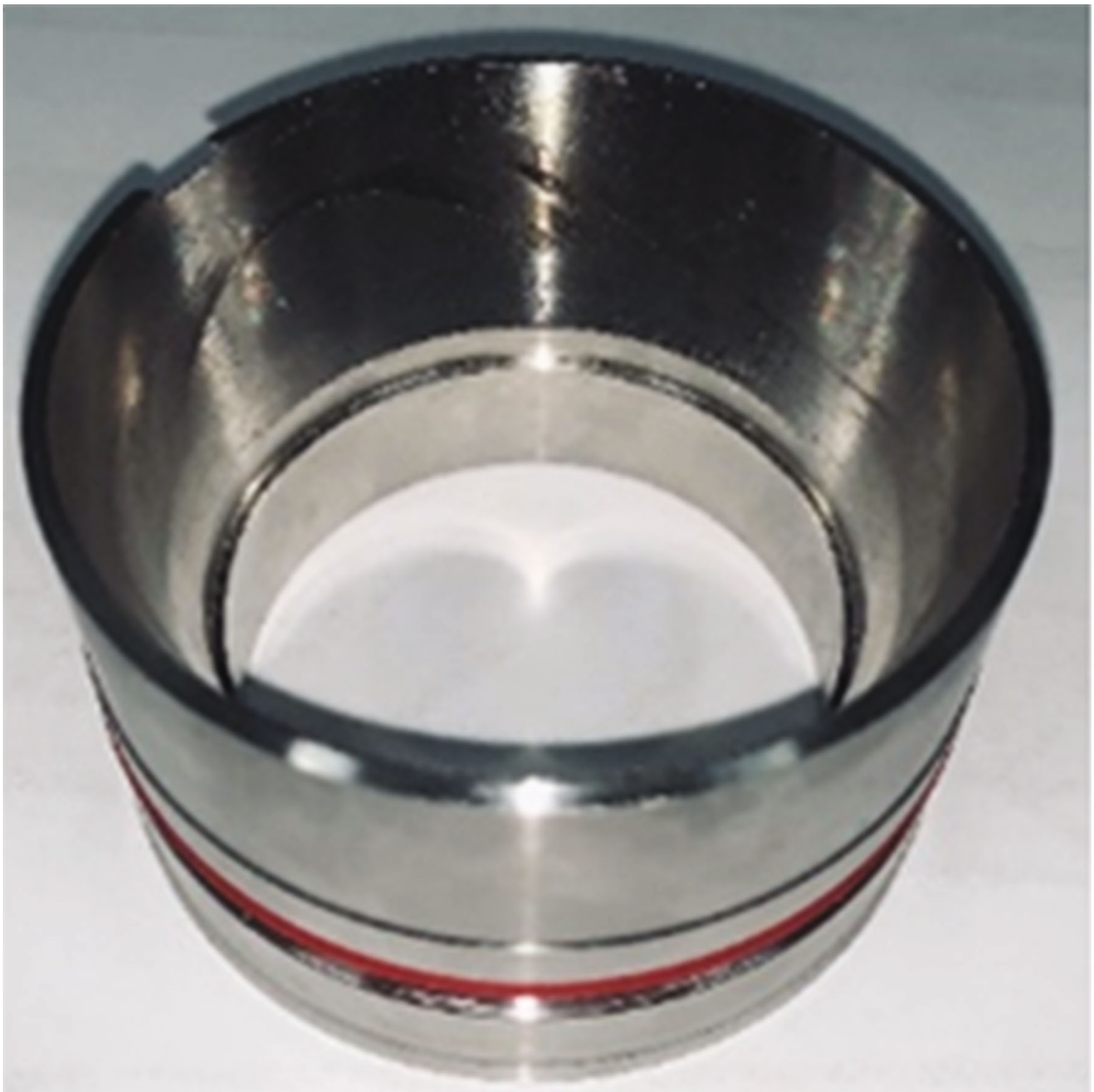

(a)

Figure 12: Continued.

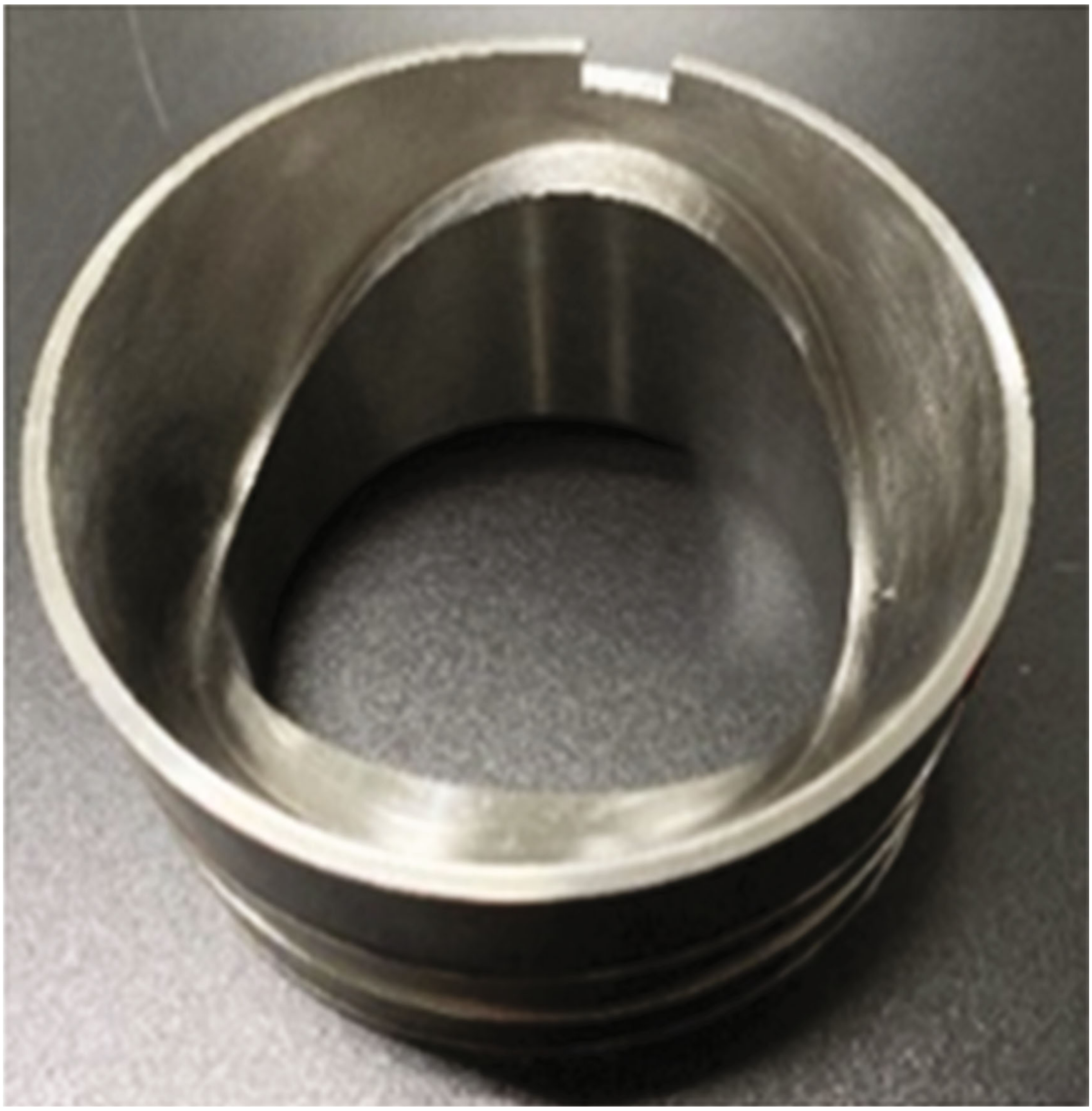

(b)

Figure 12: Experimental objects. (a) Conical sealing structure. (b) Wedge sealing structure.

following formula:

$$P_i + \frac{\rho {v_1}^2}{2} + \rho gh = P_o + \frac{\rho {v_2}^2}{2} + \rho gh. \tag{7}$$

P_0 (MPa) is the atmospheric pressure, which is negligible compared with the pressure in the pressure-maintaining tank. $T(s)$ is the time over which pressure is maintained, C_l is the fluid leakage coefficient, and $A(m^2)$ is the channel area. Because the fluid velocity inside the vessel is small, the formula can be changed as follows:

$$\frac{\Delta Q}{T} = C_l A \sqrt{\frac{\rho P_i}{2}}. \tag{8}$$

In formula (8), the area of the flow passage is the total area of fine flow passage that causes leakage through the sealing surface of the pressure-maintaining controller. As shown in Figure 6, the maximum value of the roughness profile curve of the contact surface is 5.8 μm, and the minimum value is -3.2 μM. When the bonnet is in contact with the valve seat, the height of the flow passage is approximately half of the maximum roughness, so the flow area $A(m^2)$ is calculated as follows:

$$A = \frac{kR\pi R_z}{\cos\alpha}. \tag{9}$$

Therefore, the fluid leakage rate Q_v can be expressed as follows:

$$Q_v = C_l A \sqrt{\frac{\rho P_i}{2}} = C_l \frac{kR\pi R_z}{\cos\alpha} \sqrt{\frac{\rho P_i}{2}}. \tag{10}$$

Table 2: Parameters used in the pressure leakage rate test.

Object	Group number	1	2	3	4	5	6	7	8	9	10
Test chamber	Initial pressure (MPa)	15.9	22.4	31.9	41	50	61.7	71	80.8	89.8	99.1
	Time (s)	150	150	150	150	150	150	150	150	150	150
Conical structure	Initial pressure (MPa)	5.7	14.3	20.8	25.1	30.2	35.3	40.7	45.9	0	0
	Time (s)	1-60	1-60	1-60	1-60	1-60	1-60	1-60	1-60	0	0
Wedge structure	Initial pressure (MPa)	14.9	19.6	30.6	40.3	49.1	60.4	70.6	79.6	90.6	98
	Time (s)	1-60	1-60	1-60	1-60	1-60	1-60	1-60	1-60	1-60	1-60

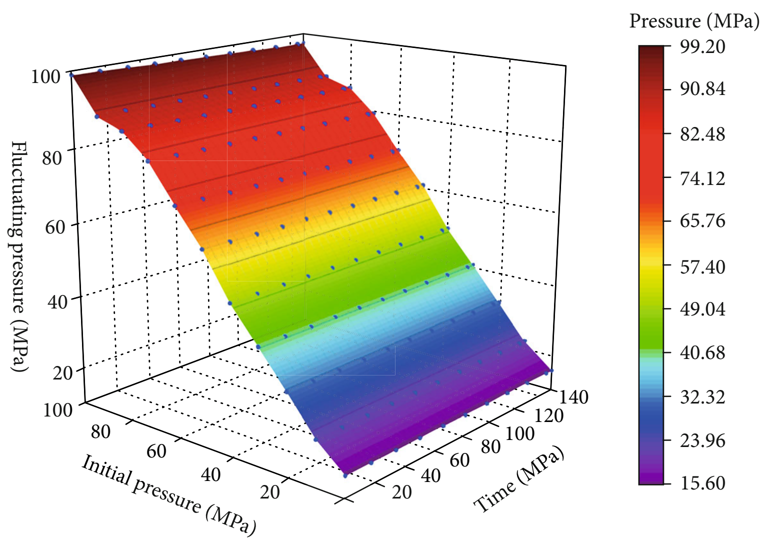

(a)

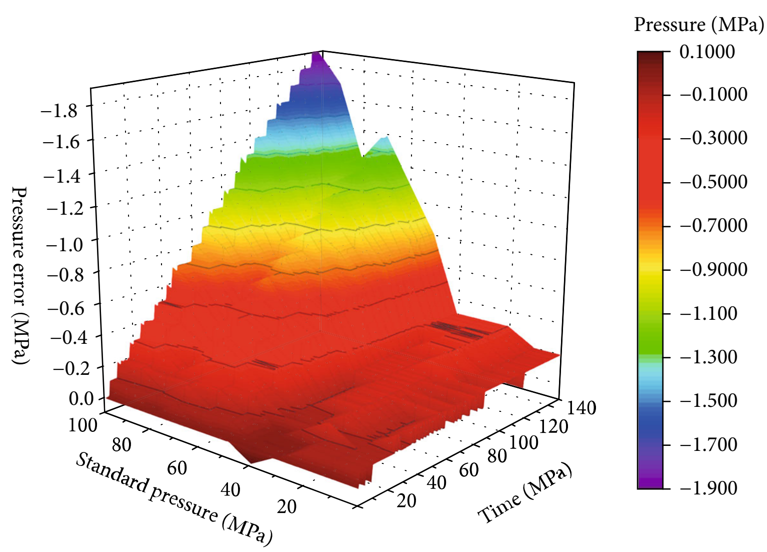

(b)

Figure 13: Test results for the test chamber. (a) Pressure-holding capacity of the high-pressure test chamber. (b) Pressure leakage rate of the high-pressure test chamber.

According to formula (10), in a stable sealing state, the higher the pressure is, the greater the pressure leakage rate is, and the pressure is exponentially related to the fluid leakage rate.

To prevent a rapid decrease in pressure caused by liquid leakage, a pressure accumulator is integrated into the coring device. As shown in Figure 7, the principle is based on the compressibility of gas to achieve a slow pressure

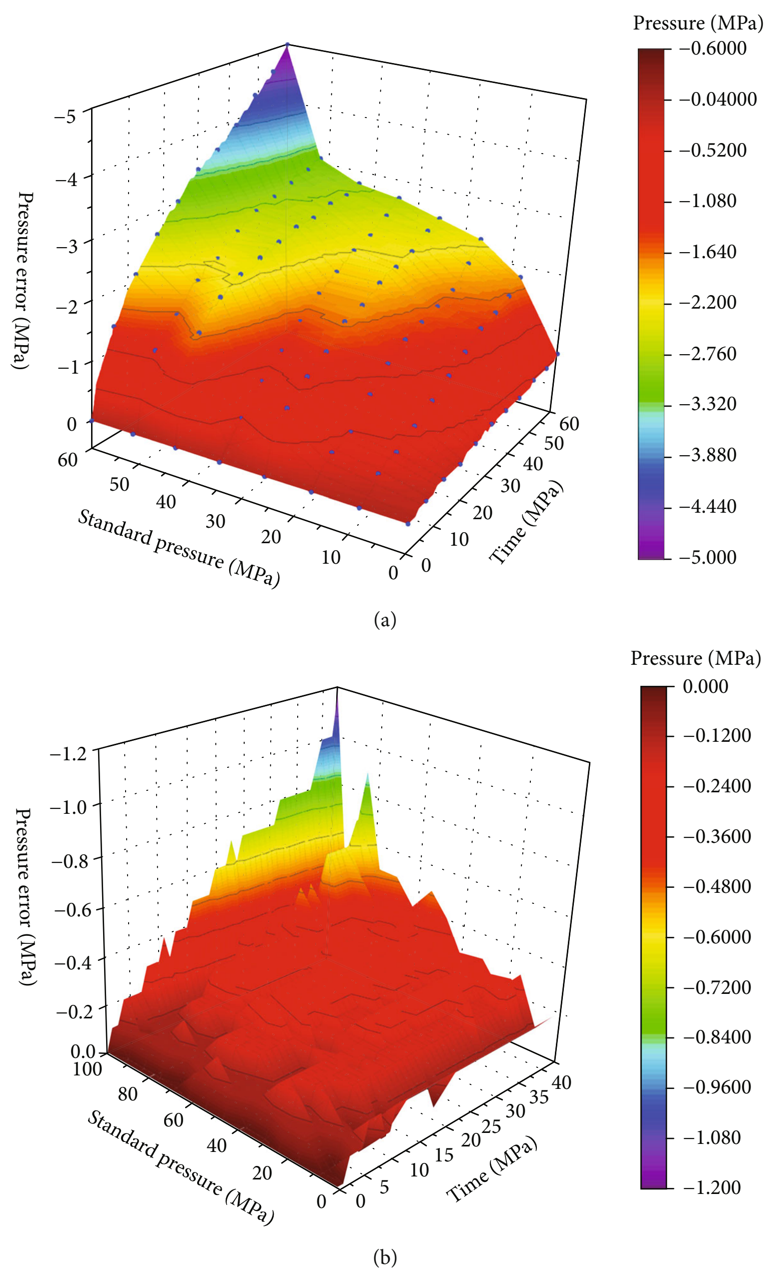

FIGURE 14: Test results for the pressure-maintaining controller. (a) Leakage rate of conical sealing. (b) Leakage rate of wedge sealing.

reduction in the chamber. Therefore, the pressure compensation rate of the pressure-retaining mechanism needs to be considered when determining the pressure-holding mechanism.

According to the gas balance equation, the following expression can be established:

$$P_1 V_1 = P_2 V_2 = nRT. \tag{11}$$

In formula (11), P_1 (MPa) and P_2 (MPa) are the pressures before and after vessel leakage, respectively; $V_1(L)$ and $V_2(L)$ are the volume changes before and after gas leakage, respectively; and T is the ambient temperature. Now, we can obtain the following formula:

$$V_2 - V_1 = \frac{nRT}{P_1} - \frac{nRT}{P_2} = nRT\frac{\Delta p}{P_1 P_2}. \tag{12}$$

When time is minimized,

$$P_1 = P_2 = P_i. \tag{13}$$

Then, formula (12) becomes

$$\Delta p = \frac{p_i^2 (V_2 - V_1)}{nRT}. \tag{14}$$

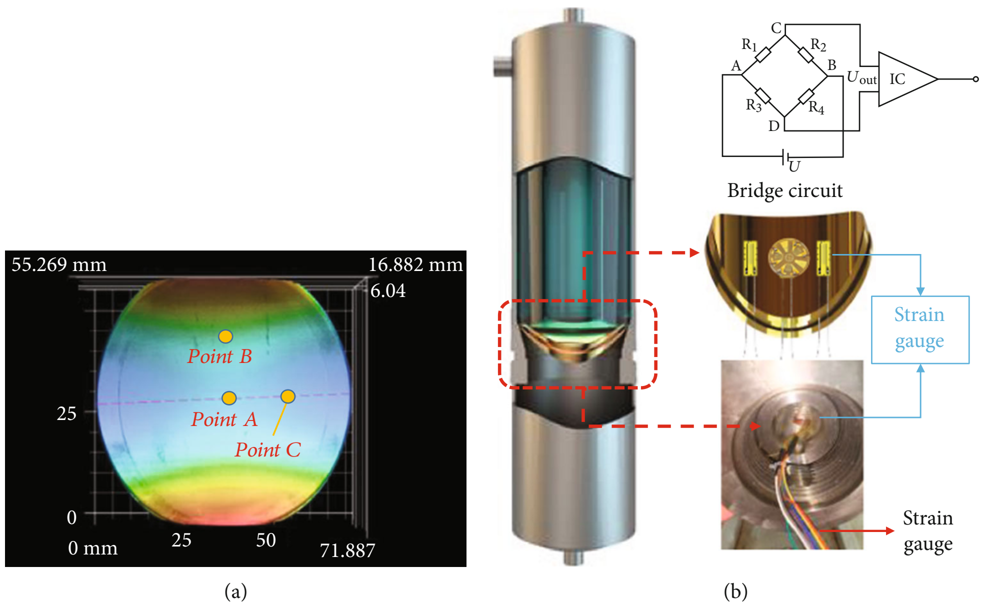

FIGURE 15: Deformation and failure pressure test. (a) 3D profile scanning analysis. (b) Test system of the pressure-maintaining controller.

Because the diameters of the gas and liquid chambers are different, the relationship between the pressure leakage rate and the pressure of the pressure-maintaining controller is as follows:

$$\Delta P_v = \frac{p_i^2 Q_v D_g^2}{nRTD_L^2} = C_l \frac{kR\pi R_z D_g^2}{nRTD_L^2 \cos\alpha} \sqrt{\frac{\rho}{2}} p_i^{2.5}. \qquad (15)$$

According to formula (15), the pressure leakage rate of the pressure-maintaining controller is exponentially related to the sealing pressure.

As shown in Figure 8, when the wire diameter of the sealing ring is compressed to the depth of the sealing groove at a high pressure, the contact surface is sealed by a rubber ring to form a metal seal. As the pressure continues to increase and exceeds the limit pressure of the pressure controller, the pressure-maintaining controller will deform, as shown in Figure 8. Additionally, the metal chimeric sealing line will be damaged, and the seal will fail. It is important to study the mechanism of seal line failure to improve the pressure-maintaining controller; this process requires exploration and theoretical verification through pressure environment reconstruction experiments involving the pressure-maintaining controller [28].

In this section, the sealing mechanism of the pressure-maintaining controller is analyzed from the time the seal is formed to the time when the seal fails at the limit pressure. To verify the theoretical results and assess the sealing principle of the pressure-maintaining controller, physical experiments must be performed.

4. Confirmatory Experiment of the Sealing and Failure Mechanisms

Figure 9 shows the physical diagram of the integrated experimental system used to assess the pressure-maintaining controller. An environment simulation chamber for the pressure-maintaining controller was built into the test chamber. The test chamber can maintain the relative stability of the experimental environment and play a protective role. A multistage variable frequency pump was placed in the ultra-high-pressure circulation system, and the pressure was controlled according to the preinput pressure curve through the pressure control system. The strain parameters of the pressure-maintaining controller were input into the upper computer through the data acquisition device, and a data chart was output after computer processing.

4.1. Experimental Verification of Seal-Form Conversion. As shown in Figure 10(a), when the pressure is low, there is no scoring on the sealing surface of the valve seat, indicating that the metal sealing stage has not been reached. As the pressure increases, the seat contact surface appears as a shallow chimeric mark, as shown in Figure 10(b). As the pressure continues to rise, a deep nick is formed on the contact surface of the pressure-maintaining controller, as shown in Figure 10(c), which indicates that the valve cover and valve seat gradually enter the metal contact sealing state at high pressure.

As shown in Figure 11, the nick is caused by the outer contour line of the valve cover squeezing the valve seat, which forms a wavy curve on the contact surface of the valve seat, resulting in a depression depth of 0.1 mm and a surface height difference of 0.2 mm. The experimental results show that the pressure-maintaining controller forms a soft seal with the rubber ring in the initial sealing stage. As the pressure gradually increases, a hard metal seal is formed, and a chimeric curve is generated between the valve cover and the valve seat, which verifies the sealing state transition and transition principle.

4.2. Leakage Rate Test at Different Initial Pressures. The pressure leakage test focuses on the conical sealing surface and

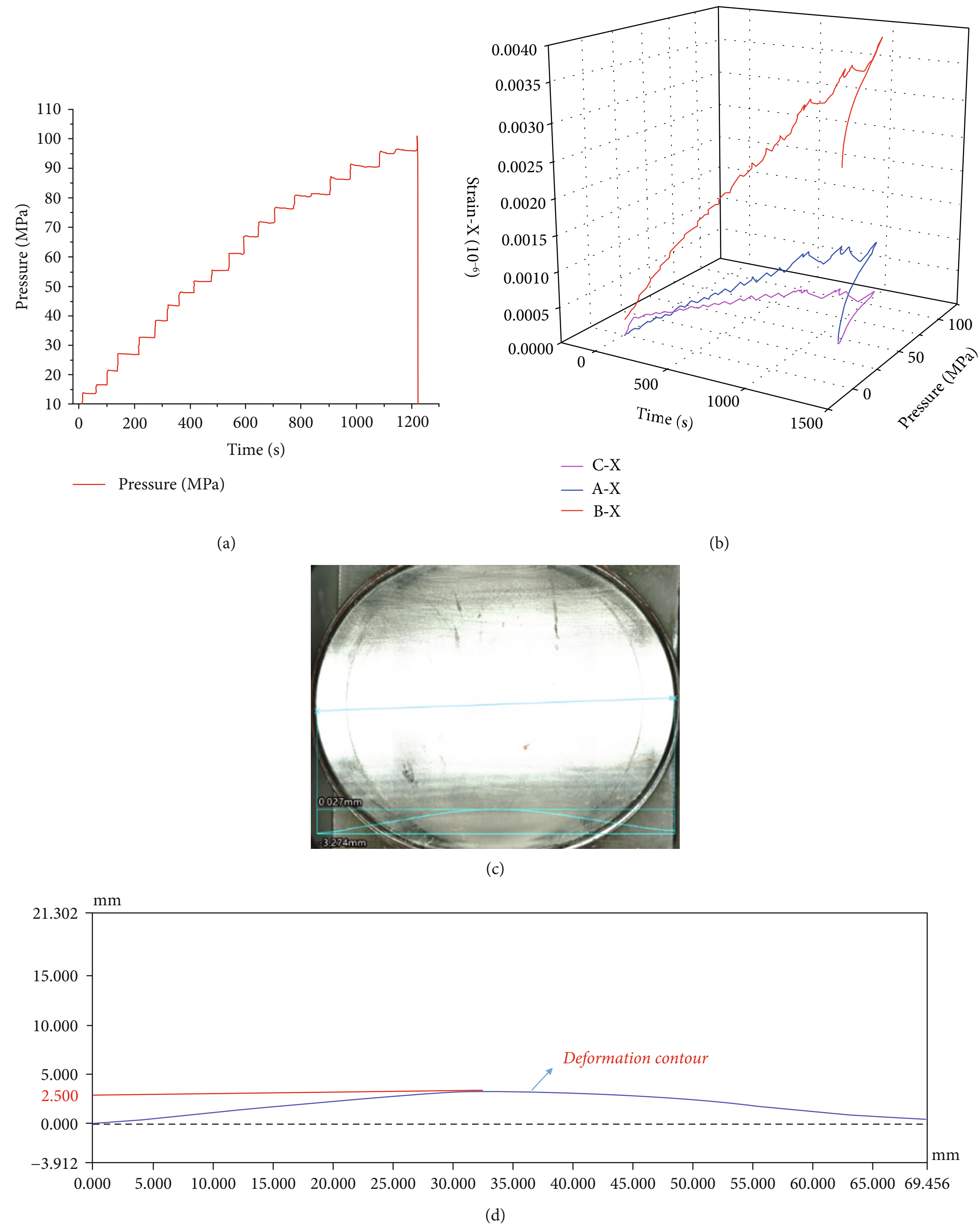

Figure 16: Test result. (a) Failure pressure loading curve. (b) Multipoint strain curve for the valve cover. (c) Contour scanning of the valve cover. (d) Contour curve of the valve cover centerline.

wedge sealing surface, as shown in Figure 12. First, the wedge sealing surface is assessed based on the pressure leakage and failure theory. Second, the stepped surface is investigated to support the deformation of the valve cover. Finally, the wedge seal forms a multistage sealing channel to reduce the pressure leakage rate.

Due to the pressure leakage and test system error, it is necessary to test the pressure capacity of the high-pressure test chamber separately before testing the pressure-maintaining controller. The test accuracy of the system can then be calibrated based on the test results. When two kinds of pressure-maintaining controllers are tested, it is necessary to ensure that the temperature, ambient pressure, pressure medium, test chamber volume, and other parameters are identical. The control pressure was the only variable in the experiments, and pressure gradient experiments were performed in 10 groups. The test parameters were set as follows in Table 2.

Since the pressure source was a high-pressure plunger pump, there was a specific deviation between the initial pressure and the set value, and this variation was 1 MPa. The experimental temperature was 25°C, and the pressure medium was water.

The holding time of the pressure-maintaining controller was set as 60 s. To correct the experimental results, the holding time of the pressure chamber was set from 0 to 150 s. Due to the limitation of the holding capacity of the cone-type pressure-maintaining controller, only eight groups of different preset pressure tests were explored. The eight groups of pressure values were set in an increasing sequence from 5 MPa to 45 MPa.

4.2.1. Calibration and Correction of the Test System. As shown in Figure 13(a), after loading to the preset pressure, the pressure in the test chamber changes little with time, and the flatness of the entire three-dimensional pressure surface over time is excellent. The pressure in the test chamber is well maintained. Therefore, the system can be used as a test platform to assess the pressure-maintaining ability of the pressure-maintaining controller.

Figure 13(b) shows the change in pressure leakage with time at each preset pressure. This result can be used to calibrate the test accuracy of the high-pressure test system. According to the experimental results, the initial offset is determined for the high-pressure test system, and the pressure value of the pressure-holding controller corresponding to the sealing time is corrected so that the measured pressure data are the real pressure capacity data.

4.2.2. Analysis of the Pressure Leakage Rate of the Pressure-Maintaining Controller. As shown in Figure 14(a), the experimental results indicate that there is a certain amount of leakage at each preset pressure. Figure 14(b) shows the leakage rate of the pressure-maintaining controller at different preset pressures. The higher the preset pressure is, the greater the pressure leakage per unit time. At each preset pressure, the leakage rate gradually decreases with time. The leakage rate of the wedge seal structure is lower than that of the cone seal structure at the same pressure, which indicates that the pressure-holding capacity of the wedge seal structure is better than that of the conical seal structure. The experimental results suggest that with increasing pressure, the pressure leakage of the pressure-maintaining controller increases gradually. This finding preliminarily verifies the leakage rate theory proposed above for the pressure-maintaining controller.

4.3. Experimental Verification of Deformation and Failure Theory. The experimental design is shown in Figure 15(b). The ultimate pressure capacity of the pressure-maintaining controller is measured through destructive experiments in the high-pressure test chamber. High-pressure deformation is measured with a multipoint strain testing system, which includes a strain gauge, data collector, and upper computer. The strain data are output to the data collector through a signal line at the bottom of the high-pressure test chamber, and the data are analyzed and processed by the upper computer.

In the high-pressure test experiment, with increasing pressure, the final seal of the valve cover fails, and the pressure rapidly decreases to 0. The deformation of the valve cover during this process is shown in Figure 16(b).

Figure 16(a) shows the deformed bonnet after the high-pressure test, and the corresponding deformation curve is shown in Figure 16(b). The results indicate that at high pressures, the bonnet and seat maintain a good fit, but the geometry of the bonnet changes with the pressure. The results of the strain test show that the bending surface of the valve cover experiences the largest deformation, and the deformation quickly causes sealing failure. This result preliminarily verifies the high-pressure deformation theory and ultimate compressive strength theory proposed above for the valve cover.

5. Conclusion

In this paper, the ability of a pressure-maintaining controller is analyzed, and the sealing principle and failure theory for a core pressure-retaining system are preliminarily established. In situ pressure simulation experiments are performed to verify the pressure-holding controller.

(1) In a deep rock coring system, the pressure environment of the core is affected by the initial sealing stability, pressure leakage rate, and ultimate pressure resistance capacity of the pressure-maintaining controller

(2) A test method for pressure-maintaining controllers, which are the key component of pressure-maintaining coring systems, is proposed, and an in situ pressure environment testing system is designed to perform pressure-holding capacity tests involving a pressure-maintaining controller

(3) The transition from a soft seal to a metal seal is verified through a metal chimeric curve experiment. The O-ring seals the initial pressure environment of the core, and when the pressure exceeds the critical point, a metal seal is formed

(4) The pressure leakage rate experiment verifies the trend of the pressure leakage rate. The results suggest that the pressure leakage of the pressure-maintaining controller increases gradually with increasing pressure

(5) The sealing failure pressure of the pressure-maintaining controller is determined based on the ultimate pressure resistance capacity and deformation test results, and the proposed high-pressure deformation theory and ultimate pressure strength theory for the valve cover are preliminarily verified

Data Availability

The raw/processed data used to support the findings of this study have not been made available because the data also forms part of an ongoing study.

Conflicts of Interest

The authors declare that they have no conflicts of interest.

Acknowledgments

This work was supported by the National Natural Science Foundation of China (grant numbers 51827901 and 51805340). The financial aids are gratefully acknowledged.

References

[1] H. P. Xie, F. Gao, and Y. Ju, "Research and development of rock mechanics in deep ground engineering," *Chinese Journal of Rock Mechanics and Engineering*, vol. 34, no. 11, pp. 2161–2178, 2015.

[2] H. P. Xie, "Research review of the state key research development program of China deep rock mechanics and mining theory," *Journal of China Coal Society*, vol. 44, no. 5, pp. 1283–1305, 2019.

[3] Z. Wen, S. Jing, Y. Jiang et al., "Study of the fracture law of overlying strata under water based on the flow-stress-damage model," *Geofluids*, vol. 2019, Article ID 3161852, 12 pages, 2019.

[4] Z. Zhang, H. Xie, R. Zhang et al., "Deformation damage and energy evolution characteristics of coal at different depths," *Rock Mechanics and Rock Engineering*, vol. 52, no. 5, pp. 1491–1503, 2019.

[5] M. Gao, Z. Zhang, Y. Xiangang, C. Xu, Q. Liu, and H. Chen, "The location optimum and permeability-enhancing effect of a low-level shield rock roadway," *Rock Mechanics and Rock Engineering*, vol. 51, no. 9, pp. 2935–2948, 2018.

[6] H. Kang, J. Wang, and J. Lin, "Case studies of rock bolting in coal mine roadways," *Chinese Journal of Rock Mechanics & Engineering*, vol. 29, no. 4, pp. 649–664, 2010.

[7] M. Z. Gao, R. Zhang, J. Xie, G. Y. Peng, B. Yu, and P. G. Ranjith, "Field experiments on fracture evolution and correlations between connectivity and abutment pressure under top coal caving conditions," *International Journal of Rock Mechanics and Mining Sciences*, vol. 111, pp. 84–93, 2018.

[8] M. Z. Gao, S. Zhang, J. Li, and H. Wang, "The dynamic failure mechanism of coal and gas outbursts and response mechanism of support structure," *Thermal Science*, vol. 23, Suppl. 3, pp. 867–875, 2019.

[9] H. P. Xie, "Research framework and anticipated results of deep rock mechanics and mining theory," *Advanced Engineering Sciences*, vol. 49, no. 2, pp. 1–16, 2017.

[10] Z. Jun and Y. Ren-Shu, "Research on mechanics propertes of the deep brittle rock with triaxial unloading experiment," *China Mining Magazine*, vol. 18, no. 7, pp. 91–93, 2009.

[11] G. R. Dickens, P. J. Wallace, C. K. Paull, and W. S. Borowski, "Detection of methane gas hydrate in the pressure core sampler (PCS): volume-pressure-time relations during controlled degassing experiments," *Proceedings of the Ocean Drilling Program: Scientific Results*, , pp. 113–126, Texas A&M University, 2000.

[12] A. V. Milkov, G. R. Dickens, G. E. Claypool et al., "Co-existence of gas hydrate, free gas, and brine within the regional gas hydrate stability zone at Hydrate Ridge (Oregon margin): evidence from prolonged degassing of a pressurized core," *Earth and Planetary Science Letters*, vol. 222, no. 3-4, pp. 829–843, 2004.

[13] G. R. Dickens, D. Schroeder, and K. U. Hinrichs, "The pressure core sampler (PCS) on ODP Leg 201: General operations and gas release," *Proceedings of the ocean drilling program, Initial Reports, vol. 201*, , pp. 1–22, Ocean Drilling Program, College Station, TX, 2003.

[14] G. R. Dickens, C. K. Paull, and P. Wallace, "Direct measurement of in situ methane quantities in a large gas-hydrate reservoir," *Nature*, vol. 385, no. 6615, pp. 426–428, 1997.

[15] H. Amann, H. J. Hohnberg, and R. Reinelt, "HYACE-a novel autoclave coring equipment for systematic offshore gas hydrate sampling," *Deutsche Wissenschaftliche Gesellschaft für Erdgas und Kohle eV (DGMK), Report 9706*, DGMK-Tagungsbericht, 1997.

[16] K. Masayuki, U. Satoru, and Y. Masato, "Pressure temperature core sampler (PTCS)," *Journal of the Japanese Association for Petroleum Technology*, vol. 71, no. 1, pp. 139–147, 2006.

[17] M. Matsuzawa, S. Umeza, and K. Yamamoto, "Evaluation of experiment program 2004: natural hydrate exploration campaign in the Nankai-Trough offshore Japan," in *IADC/SPE Drilling Conference*, Miami, Florida, USA, February 2006.

[18] Z. Shuai, D. Sier, Z. Wenhu, and K. Naizheng, "Simulation and experiment on sealing mechanism with rigid-flexible combined seal groove in hub bearing," *Tribology International*, vol. 136, pp. 385–394, 2019.

[19] L. Peng, S. Wen-Jie, J. Qing-Lin, and L. Xin-Juan, "Sealing performance of O-ring in deep sea high pressure environment," *Chinese Hydraulics & Pneumatics*, no. 4, 2017.

[20] L. I. Farfán-Cabrera, E. A. Gallardo-Hernández, J. B. Pascual-Francisco, C. D. Resendiz-Calderon, and C. Sedano de la Rosa, "Experimental method for wear assessment of sealing elastomers," *Polymer Testing*, vol. 53, pp. 116–121, 2016.

[21] X. Peng, X. Mao, D. Gao et al., "Experimental study of a remote sealing method for vacuum leak," *Vacuum*, vol. 114, pp. 41–43, 2015.

[22] X. Wang, Z. Wen, Y. Jiang, and H. Huang, "Experimental study on mechanical and acoustic emission characteristics of rock-like material under non-uniformly distributed loads," *Rock Mechanics and Rock Engineering*, vol. 51, no. 3, pp. 729–745, 2018.

[23] Z. J. Wen, X. Wang, Y. Tan, H. Zhang, W. Huang, and Q. Li, "A study of rockburst hazard evaluation method in coal mine," *Shock and Vibration*, vol. 2016, Article ID 8740868, 9 pages, 2016.

[24] Z. Q. He, L. Chen, T. Lu, and J. Xie, "The optimization of pressure controller for deep earth drilling," *Thermal Science*, vol. 23, Suppl. 3, pp. 877–885, 2019.

[25] C. Sieben and G. Reinhart, "Development of a force-path prediction model for the assembly process of o-ring type seals," *Procedia CIRP*, vol. 23, pp. 223–228, 2014.

[26] L. Shi, K. Wang, D. Feng, H. Zhang, and P. Wang, "Wellbore trajectory control tool seal system leakage analysis based on steady gap flow," *Advances in Mechanical Engineering*, vol. 12, no. 6, Article ID 168781402093046, 2020.

[27] H. Zhao, H. Su, and G. Chen, "Analysis of total leakage of finger seal with side leakage flow," *Tribology International*, vol. 150, article 106371, 2020.

[28] Z. P. Liu, J. X. Zhao, G. J. Ma, X. F. Gao, and L. Jiang, "Exhausted jet caused the deformation of front metal seal covers in a multiple launch rocket system," *Journal of Physics: Conference Series*, vol. 1507, no. 3, article 032018, 2020.